J. Membrane Biol. 153, 1–11 (1996)

The Journal of
Membrane
Biology

Hydraulic Properties of MDCK Cell Epithelium

M.M. Timbs, K.R. Spring
Laboratory of Kidney and Electrolyte Metabolism, National Heart, Lung and Blood Institute, NIH, Bethesda, MD 20892-1598

Received: 10 January 1996/Revised: 9 May 1996

Abstract. The water permeability of the apical and basolateral cell membranes and the compliance of the lateral intercellular spaces (LIS) of MDCK monolayers were measured on confluent cultures grown on permeable supports. Cell membrane water permeabilities were determined, using quantitative differential interference light microscopy, from the rate of cell volume decrease after exposure to a hyperosmotic bathing solution. Both membranes exhibited osmotic water permeabilities (P_{OSM}) of ~10 μm/sec, comparable to that of unmodified lipid bilayers. The compliance of the cell membranes forming the lateral intercellular space (LIS) between cells was determined from the pressure-volume relation. Confocal microscopy of fluorescent labeling of the basolateral cell membranes was used to delineate the LIS geometry as transepithelial hydrostatic pressure was varied. The LIS were poorly deformable as a function of transepithelial hydrostatic pressure until a pressure of ⩾8 cm H_2O (basolateral > apical) was reached where catastrophic failure of intercellular connections occurred. The compliance of the LIS was calculated from the geometry changes at pressures <8 cm H_2O and ranged from 0.05–0.11 cm H_2O^{-1}, comparable to that previously predicted in mathematical models of the rat proximal tubule.

Key words: Water permeability—Compliance—Confocal microscopy—Cell volume—Fluorescence

Introduction

The lateral intercellular spaces (LIS) between epithelial cells are the putative site of solute and water coupling in isosmotic fluid transporting epithelia (Whitlock & Wheeler, 1964; Diamond & Bossert, 1968). Recent investigations from our laboratory have elucidated the ionic composition of the LIS of MDCK cell monolayers (Harris et al., 1994; Chatton & Spring, 1995; Xia, Persson, & Spring, 1995) as well as the sodium and chloride fluxes across the tight junctions and cells (Kovbasnjuk et al., 1995; Xia et al., 1995). The pathways for water flow across the MDCK epithelium have not been similarly investigated. In the present study, some of the relevant hydraulic properties of MDCK monolayers are characterized.

The apical and basolateral cell membrane water permeabilities are important parameters in all mathematical models of water flow across an epithelium. The transcellular water permeability is usually calculated as the serial sum of the experimentally measured apical and basolateral cell membrane water permeabilities. The water permeability of the individual cell membranes of MDCK cells has not been previously determined, although estimates of transepithelial water permeability of MDCK cell cysts have been made (Mangoo-Karim & Grantham, 1990; Tanner, Maxwell, & McAteer, 1992). In the present study, the water permeabilities of the cell membranes were calculated from the rate of osmotically induced cell shrinkage using images obtained by differential interference contrast microscopy.

Previous experimental investigations of the morphology of rabbit gallbladder epithelium showed substantial dilation of the LIS during fluid transport and collapse after cessation of active solute transport (Tormey & Diamond, 1967; Spring & Hope, 1978). The dilation was presumed to be indicative of the hydrostatic pressure difference developed by active solute extrusion into the LIS. In our recent studies, we noted that the LIS of MDCK cell monolayers did not collapse when active transport was inhibited by ouabain (Chatton & Spring, 1995; Kovbasnjuk et al., 1995; Xia et al., 1995). The significance of the lack of LIS collapse during transport inhibition could not be assessed without knowledge of the compliance of the LIS of MDCK cells. The only

Correspondence to: K.R. Spring

published LIS compliance data were derived from pressure-volume curves obtained on *Necturus* gallbladder epithelium (Spring & Hope, 1978). Although these results showed a highly deformable compartment, no comparable information is available for any mammalian epithelium.

Mathematical models of the rat proximal tubule with a moderately deformable (compliant) LIS gave the best fit to experiments in which peritubular oncotic forces were allowed to vary (Weinstein, 1984). The pressure-volume relation of the LIS of the rat proximal tubule used to calculate the compliance of the walls was proposed by Huss and Marsh (1975) with an elastic, thin-walled tube as a model system.

To study the compliance and temporal stability of the LIS of MDCK cells, we employed confocal fluorescence microscopy methods developed in our laboratory. The LIS of cells growing on permeable supports were loaded with fluorescent dyes both as described previously (Chatton & Spring, 1994) and by the introduction of fluorescently labeled lipids into the membranes of cells. Images of the fluorescently labeled LIS were used for the determination of LIS shape and pressure-volume characteristics.

Materials and Methods

Cell Culture

Low resistance MDCK cells, passage 64–76 from the American Type Culture Collection (Rockville, MD) were cultured as previously described (Harris et al., 1994) using Dulbecco's modified Eagle medium (DMEM) and 2 mM glutamine without added riboflavin, antibiotics and phenol red. The culture medium for stock cells was supplemented with 10% fetal bovine serum (Gibco, Grand Island, NY).

The cells were grown to confluence on 24 mm Anocell membranes (Whatman, Clifton, NJ) in DMEM supplemented with 5% fetal bovine serum for 5–12 days. Before seeding the cells, the filters were treated with medium containing 5% fetal bovine serum for 5 min at 37°C, the medium was removed, and the filters exposed to ultraviolet light for 1–2 hrs.

Experimental Solutions and Perfusion System

HEPES-buffered experimental solutions contained (mM): 142 Na^+, 5.3 K^+, 1.8 Ca^{2+}, 0.8 Mg^{2+}, 137 Cl^-, 0.8 SO_4^{2-}, 14 HEPES, 5.6 glucose. The HEPES solutions were gassed with room air and their pH was adjusted to 7.4 at 37°C.

Chemicals

BCECF [2′,7′-bis (carboxyethyl)-5 (6)-carboxyfluorescein], H-110 [5-(N-hexadecanoyl) aminofluorescein], D-109 [5-(N-dodecanoyl) aminofluorescein], $diIC_{16}(3)$ [1,1′-dihexadecyl-3,3,3′,3′-tetramethylindocarbocyanine perchlorate], fluorescein DHPE [N-(5-fluoresceinthiocarbamoyl)-1,2,-dihexadecanoyl-sn-glycer-3-phosphoethanolamine, triethylammonium] were obtained from Molecular Probes (Eugene, OR).

Confocal Fluorescence Microscopy

The dependence of LIS size and volume on transepithelial hydrostatic pressure difference was analyzed from confocal images of the fluorescence of the dye-loaded LIS or fluorescently labeled adjacent cell membranes. The cells were illuminated at 488 nm with an incident light flux of 40 $\mu W/cm^2$ measured at the back focal plane of the objective lens. Optical sections of the LIS were obtained at 0.25–1 μm intervals from the basal surface to the tight junction. LIS were selected which were oriented along the optical axis and did not undergo substantial shifts during alterations in transepithelial hydrostatic pressure difference. These experiments were performed on the stage of an inverted microscope (Diaphot, Nikon, Melville, NY) equipped with a confocal attachment (Odyssey, Noran, Middleton, WI) modified for simultaneous transmitted light DIC and low light level fluorescence (Nitschke & Spring, 1995). The cell monolayers were observed with a 100×/1.3 N.A. objective lens (Nikon). The images were digitized and stored on disk for subsequent offline analysis. The sequence of events (e.g., solution valves, video gain, illumination intensity, focus position) during the experiment was controlled by a computer using customized software (Image-1, Universal Imaging, West Chester, PA).

For generation of the pressure-volume curves, optical sections were taken at 1 μm focal displacements from the level of the tight junction to the base of the LIS at the level of the permeable support. Each image was the average of 16 video frames and took 0.5 sec to acquire. A complete series of optical sections required about 2.5–5 seconds depending on the LIS height. Transepithelial hydrostatic pressure gradients were imposed by adjusting the height of the perfusion reservoirs to the desired pressure difference and clamping the perfusion chamber outlet tubes shut to allow for pressure equilibrium throughout the system.

Differential Interference Contrast Microscopy

High resolution images of the cells and adjacent LIS were obtained by the use of differential interference contrast (DIC) imaging of monolayers grown on permeable supports and perfused at 37°C on the stage of the confocal microscope. Optical sections of MDCK cells and adjacent LIS were made at 1 μm focus displacements. The images were stored on optical disc (TQ-2031F, Panasonic), and analyzed by a program designed to automatically detect cell boundaries and to measure cell size and shape (Marsh, Jensen & Spring, 1985). Cell volume was calculated from the product of the measured areas of the optical sections and the known focus displacements as previously described (Marsh et al., 1985).

Dye Loading

BCECF (10 μM) was loaded into the LIS of cells grown on a modified permeable support from the apical bath as previously described (Chatton & Spring, 1994). Solutions of the lipidic dyes, H-110, D-109, DHPE in ethanol (5 mg/ml) were added to the basolateral bathing solution to give a final dye concentration of 20–25 μM. After dye loading for 20 min at 37°C, the cells were transferred to a culture dish containing 1 ml of HEPES-buffered perfusion solution. The basolateral bath was then exchanged three times with 1 ml of room temperature HEPES-buffered perfusate. The preparation was then transferred to a perfusion chamber and warmed to 37°C on the microscope stage. To facilitate incorporation of $diIC_{16}$ (3) and fluorescein DHPE into cell

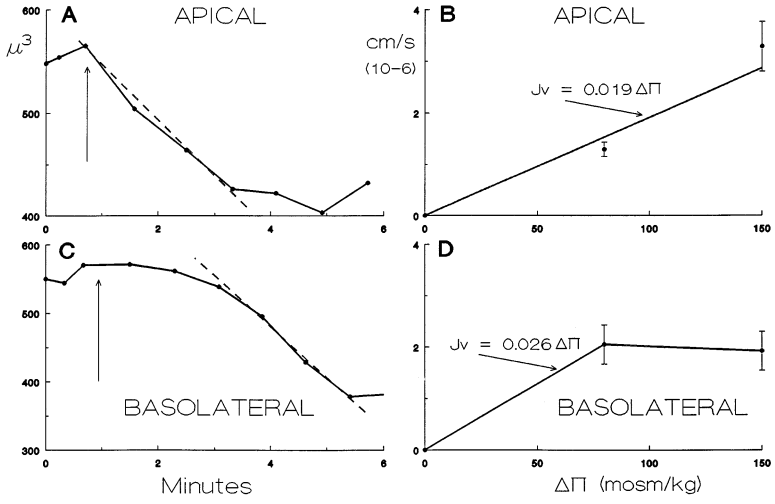

Fig. 1. Panels *A* and *C* show cell volume in μm^3 as a function of time when the indicated bathing solution osmolality was suddenly increased by 80 mOsm/kg H_2O (arrow). The broken lines depict the linear least-squares fit to the first four data points after the solution change. The opposite bathing solution remained unchanged at 300 mOsm/kg H_2O. Panels *B* and *D* depict the transmembrane volume flow, J_v, in cm/sec × 10^{-6} as a function of the imposed osmotic gradient, $\Delta\pi$, in mOsm/kg H_2O. The line in panel *B* is the best fit to the data with a zero intercept. The slope, 0.019 cm/sec-mOsm, represents the L_p. L_p was similarly determined for the results in Panel *D* for the 80 mOsm/kg H_2O gradient data only.

membranes, loading was done in the presence of 0.025% Pluronic (Molecular Probes).

Spectral Scanning

Excitation and emission spectra of all dyes used in the study were obtained in control Ringer solution in a spectrofluorimeter (FluoroMax, Spex, Edison, NJ). The emission spectrum of H-110 was also obtained in the confocal microscope using a liquid crystal tunable filter as previously described (Nitschke & Spring, 1995). The filter had a 25–30 nm bandwidth at the analyzed wavelengths. Intensity values were obtained at 10-nm intervals of emission wavelength from 515 to 605 nm.

Perfusion Chamber

The filters with adherent cells were loaded into a perfusion chamber as described previously (Chatton & Spring, 1994). Perfusion rates in both apical and basolateral baths were adjusted to be comparable at about 10–12 μl/min. The volume of each bath in the perfusion chamber was about 1 μl; 95% exchange of either bath took about 5 sec.

Analysis of Fluorescence Microscopy Images

Images were processed with the Image-1 software to separate the bright LIS from the dark cellular regions by creating a binary image after threshold determination. LIS fluorescence was measured at each pressure in a one- or two-cell region for at least five images in a field of view. A single representative image was then selected for establishment of a threshold value for the entire series. Relative LIS area was calculated using the most basolateral cross sectional area of a region of interest as the reference. Relative LIS volume was calculated by multiplying the area of the region of interest by the optical section thickness (1 μm) and normalizing the resultant volume to that determined in the absence of a transepithelial hydrostatic pressure difference.

Statistics

Data are presented as means ± SE. Statistical significance was determined using the paired or unpaired *t* test and a *P* value <0.05 was considered significant.

Results

The experiments were designed to determine the water permeability of the apical and basolateral membranes of MDCK cells as well as the pressure-volume curves of the LIS.

Cell Membrane Water Permeability

The cell membrane water permeabilities were calculated from the rate of cell volume decrease in the presence of a hypertonic perfusate. Figure 1 shows typical results of adding 80 mOsm of mannitol to either the apical (Fig. 1*A*) or basolateral perfusate (Fig. 1*C*) of MDCK cells grown on a permeable support. The opposite bathing solution remained at 300 mOsm/kg H_2O. When the apical perfusate was made hypertonic by 80 mOsm, average cell volume decreased by 13.8 ± 1.7% (Table). The predicted shrinkage of a perfect osmometer is 26.7% for this osmotic challenge. Thus, the observed shrinkage was 52% of the theoretical maximum. The less than ideal volumetric response to the osmotic challenge is typical of epithelia with a significant basolateral membrane water permeability (Strange & Spring, 1987).

As can be seen in Fig. 1*A*, cell volume decreased promptly after the osmolality increase, and the initial rate of shrinkage could be adequately estimated from a linear least-squares fit of the first few data points (broken line in Fig. 1*A*). When the osmotic gradient was increased to 150 mOsm/kg H_2O, the magnitude of the shrinkage was increased to 20.2 ± 2.8% while the rate of shrinkage more than doubled (Table). Figure 1*B* plots, on the ordinate, the rate of osmotically induced volume flow out of the cell across the apical membrane, assuming an average smooth apical membrane surface area of 57.2 μm^2 cell, as a function of the imposed osmotic gradient ($\Delta\pi$) on the abscissa. The fitted line has a slope equal to the

Table. Volume flows and water permeabilities of the cell membranes

Side of solution change (osmotic gradient mOsm/kg)	Volume flow ($\times 10^{-6}$ cm/sec)	Volume change (%)	P_{osm} μm/sec
Apical (80)	1.29 ± 0.14(10)*	13.8 ± 1.7	8.9
Apical (150)	3.28 ± 0.48(6)	20.2 ± 2.8	12.1
Basolateral (80)	2.05 ± 0.38(10)	17.5 ± 1.6	14.2
Basolateral (150)	1.92 ± 0.38(3)	45.0 ± 1.5	7.0

* Number of cells studied is indicated in parenthesis; no more than two cells were analyzed from each culture. Volume flow and P_{osm} across both the apical and basolateral cell membranes are expressed as a function of smooth apical membrane surface area.

hydraulic water permeability of 1.9×10^{-8} cm^3/cm^2-sec-mOsm, equivalent to an osmotic water permeability, P_{OSM}, of 10.6 μm/sec.

When similar experiments were performed to determine the water permeability of the basolateral cell membrane, the hyperosmotic solutions were introduced into the basolateral perfusate while the apical bath remained at 300 mOsm/kg H_2O. As shown in the experiment of Fig. 1*B*, an increase in the osmolality of the basolateral bath of 80 mOsm resulted in a 17.5 ± 1.6% cell shrinkage which is about 66% of that theoretically expected. The onset of shrinkage was delayed somewhat compared to that observed when the apical perfusate was altered, presumably reflecting the influence of the unstirred layer constituted by the 45 μm-thick permeable support. Application of a 150 mOsm/kg H_2O basolateral hypertonic gradient resulted in a 45 ± 1.5% shrinkage ($n = 3$), or 90% of that theoretically expected for a perfect osmometer.

The rate of volume flow across the basolateral membrane as a function of the osmotic gradient is shown in Fig. 1*D*. The flow rate with the 150 mOsm gradient was not significantly different from that with the 80 mOsm gradient (Table). This is consistent with the rate-limiting effect of the unstirred layer of the permeable support. The volume flow across the basolateral membrane of the cell can be calculated both as a function of the smooth apical cell membrane surface area for purposes of comparison to that of the apical membrane of the cell or as a function of the smooth basolateral membrane area. The volume flow across the basolateral membrane induced by an 80 mOsm/kgH_2O gradient, calculated with reference to the apical cell membrane area, was $2.05 \pm 0.38 \times 10^{-6}$ cm/sec, about 1.6 time that across the apical membrane with a similar osmotic gradient (Table). The calculated osmotic water permeability (P_{OSM}) was 14.2 μm/sec, about 1.33 times the average value for the apical membrane. When the 4–5 times larger smooth surface area of the basolateral membrane is taken into account, the basolateral membrane osmotic water permeability is 3.6 μm/sec, only about 40% of that of the apical membrane.

Temporal Stability of LIS Geometry

LIS were loaded with the fluorescent dye, BCECF, as previously described (Chatton & Spring, 1994) and optical sections were obtained in the confocal microscope. Figure 2 shows a series of optical sections obtained at 0.25 μm focus displacements of the dye-filled LIS. The complex folded surface and multitude of small gaps presumably reflect the high incidence of cell-to-cell connections in MDCK cells (Wacker et al., 1992).

Modest bleaching of the BCECF filling the LIS occurred during the image capture period. To evaluate the extent of bleaching, a field of cells with dye-filled LIS was illuminated with 488 nm laser light through a 100×, 1.32 N.A. objective lens continuously for 20 min. The illumination intensity was 40 $\mu W/cm^2$, measured at the back focal plane of the objective lens. Figure 3 shows both linear and semilogarithmic plots of LIS fluorescence as a function of time during continuous illumination. The bleaching rate constant under these conditions was 0.14 min^{-1}, equivalent to 0.2% decrease in intensity per second of laser illumination. A typical experimental series required 2.5–5 seconds, so the predicted bleaching would be 0.5–1.0%.

To test for spontaneous fluctuations in LIS geometry during the course of a normal experimental period (about 1 hr), confocal images of BCECF-filled LIS were captured at regular intervals. In the first group of experiments, a series of optical sections at 1-μm intervals were obtained every 10 min for a period of 40–60 min. Figure 4 shows a representative 3-D image set from a total of seven experiments in which no significant change in LIS cross-sectional area occurred. The change in LIS cross-sectional area over time averaged 4.5 ± 2.5%, not significantly different from zero. In a second series of three experiments designed to detect more rapid changes in LIS geometry, images were obtained at 1-min intervals for 6 min. Again, no statistically significant changes in geometry were observed. We concluded that LIS geometry was stable during a typical experimental period and that changes observed subsequent to alterations in trans-

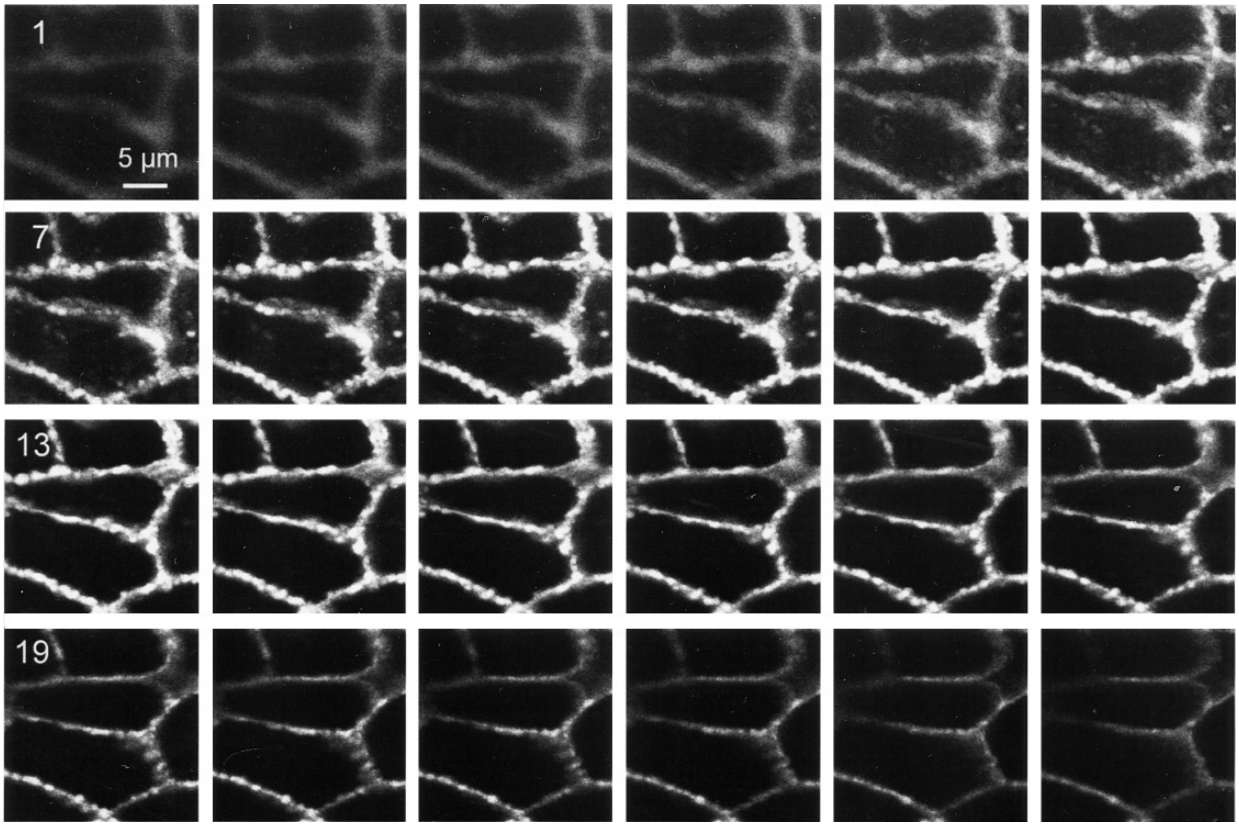

Fig. 2. Optical sections of MDCK cell monolayers, grown on a coverglass, taken with a confocal microscope (Noran Odyssey) at 0.25 μm focus displacements. The LIS were filled with the fluorescence dye BCECF by diffusion across the tight junctions. Sections are numbered in the basal (1) to the apical (24) direction. LIS begin to come into focus about at section 6 and the tight junctional end of the LIS is situated at about sections 19 to 22.

epithelial hydrostatic pressure were not due to spontaneous fluctuations of cell-to-cell connections.

Fluorescent Dye Labeling of Basolateral Cell Membrane

Several lipophilic dyes were evaluated for their utility in staining the basolateral membranes of MDCK monolayers grown on permeable supports. H-110 readily labeled the basolateral membranes only when added to the basolateral bathing solution. D-109 labeled both apical and basolateral membranes when added to the basolateral bath. $DiIC_{16}$ failed to label the basolateral membranes when added to the basolateral bath, but strongly labeled apical membranes when added to the apical bath. Addition of the detergent Pluronic (0.025%) somewhat improved basolateral labeling with $diIC_{16}$ (3), but the fluorescence was very weak. DHPE resulted in virtually no useful staining of either membrane. All subsequent experiments employing lipophilic dyes were done with H-110.

Spectrum of H-110 in the Basolateral Membrane

Figure 5 shows the emission spectrum of H-110 obtained in buffer in the spectrofluorimeter (cuvette) and in the LIS of a MDCK cell monolayer obtained in the confocal microscope. The substantial red shift of the dye in the cell membrane is consistent with a lipophilic environment and serves to confirm dye localization in the lateral cell membranes. Subsequent imaging using H-110 was done with the emission wavelength filter centered about 535 nm.

Pressure-Volume Curves of the LIS

The cross-sectional area of selected focal planes within the LIS was estimated from the confocal images of the fluorescently labeled LIS using H-110 to stain the adjacent basolateral cell membranes as described above. Figure 6 shows a representative plot of LIS area vs. applied transepithelial hydrostatic pressure (basolateral > apical) at three focal planes—at the base of the LIS, in the middle and at the plane closest to the tight junctions.

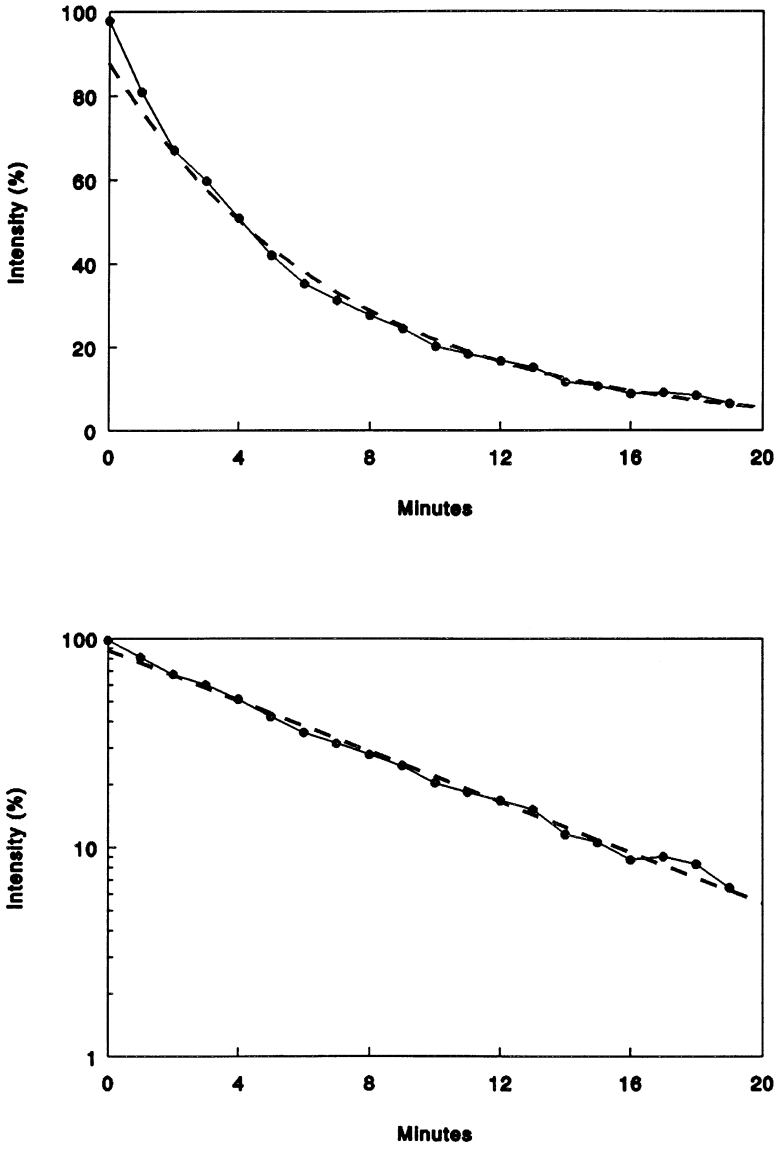

Fig. 3. Photobleaching of BCECF-filled LIS during continuous illumination of the entire field of view (40 × 40 μm) using a 100×, 1.32 NA objective lens and 488 nm laser light. The incident light flux of 40 μW/cm^2 at the back aperture of the objective lens resulted in 4 μW entering the lens and was equivalent to an illuminance of 286 mW/cm^2 at the image plane. The photobleaching curves depict the relative intensity of LIS fluorescence as a function of time in linear (top) or semilogarithmic (bottom) plots. The broken lines are fitted to the data by the method of least squares according to the equation: Intensity = 87.7 e^{-kt}, where t has the units of minutes and k = 0.14 min^{-1}. The correlation coefficient for the fit was 0.997.

As shown in Fig. 6, all three sections showed very little change in area until a basolateral-to-apical transepithelial hydrostatic pressure of 8 cm H_2O was reached. At this pressure, a sudden dramatic widening of the LIS occurred at all focal planes. Cell and LIS height remained unchanged until the critical pressure gradient of ⩾8 cm H_2O was achieved. At this point, cell detachment and gross geometric distortion of the cells and LIS often resulted.

In seven experiments in which the basolateral-apical bath hydrostatic pressure was increased by 2–4 cm H_2O, LIS cross-sectional area near the tight junction was significantly greater than the control by 22 ± 4%. At higher pressures, i.e., 8 cm H_2O, substantial widening of the entire LIS occurred in four out of five experiments. The largest increase in cross-sectional area occurred adjacent to the tight junction. This is consistent with the failure of the structural integrity of the cell-to-cell bridges spanning the LIS. The increase at the tight junctional end of the LIS amounted to 3.3 ± 1.2 fold (n = 5) at basolateral-apical pressure differences > 8 cm H_2O.

When the hydrostatic pressure difference was reversed so that the pressure in the apical bath exceeded that in the basolateral bath by 8 cm H_2O, LIS cross-sectional area was not significantly altered. The average area change of the LIS at all focal planes was −11.4 ± 4.3% (n = 5), not significantly different from zero.

Although the magnitudes of the LIS area changes resulting from imposition of modest transepithelial hydrostatic pressure gradients were small, it was possible to construct an average pressure-volume curve for the MDCK LIS. Figure 7 shows such a curve for pressure

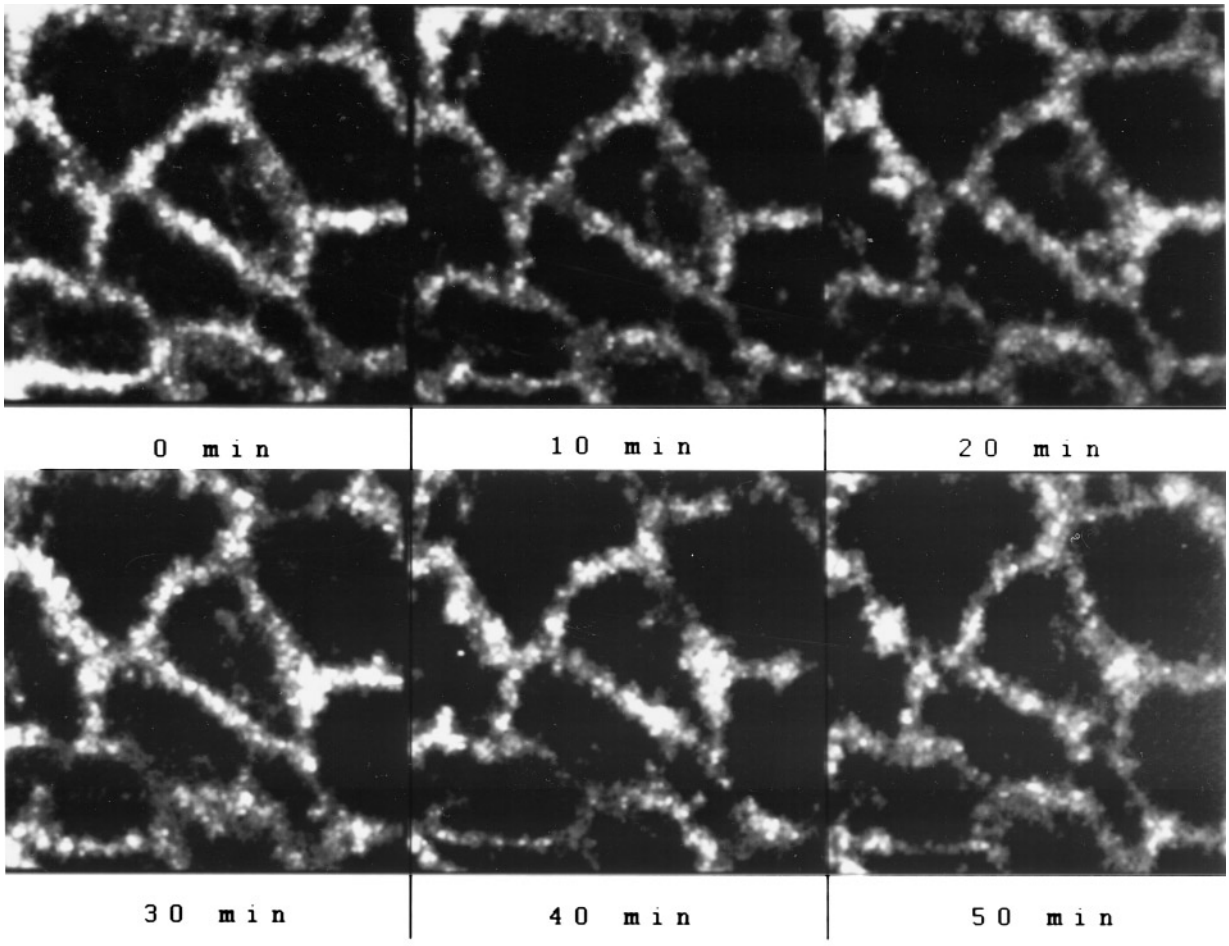

Fig. 4. Temporal stability of LIS geometry over a 50-min period was determined from five sets of optical sections at 10-min intervals of the BCECF-filled LIS of cells grown on glass coverslips. Each image depicts a 3-D projection of a stack of optical sections taken at 1 μm focus displacements. The decrease in intensity is due both to photobleaching and to diffusional loss of the dye from the LIS.

differences (basolateral-apical) ranging from −8 cm H_2O to +8 cm H_2O. The relative LIS volume at each pressure difference was estimated from the change in cross-sectional area at each focal plane relative to that of the largest area (i.e., the most basal slice) under control conditions. The area of each focal plane was determined from the pixel count in the threshold region. The data are well fitted ($r = 0.992$) by a fourth degree polynomial.

As shown previously (Huss & Marsh, 1975; Weinstein, 1984) the pressure-volume curve of a thin-walled elastic tube serves as reasonable model of the LIS. The relevant equation is:

$$\mathrm{Vol}/\mathrm{Vol}_{MAX} = 1/(1 + \alpha e^{-\beta \Delta P}) \quad (1)$$

The stiffness of the wall can be estimated from coefficient β, while the parameter α describes the relative LIS volume at 0 ΔP. The entire pressure-volume curve in Fig. 7 cannot be described by a single curve in the form of Eq. 1. For the data from −8 to +2 cm H_2O, $\alpha = 0.3$ and $\beta = 0.05$ cm H_2O^{-1}; from 0 to +6 cm H_2O, $\beta = 0.11$ cm H_2O^{-1}. At pressures above 6 cm H_2O, Eq. 1 cannot fit the data.

Discussion

This investigation is concerned both with the water permeability of the apical and basolateral membranes of MDCK cells and the compliance of the cell membranes forming the lateral intercellular spaces. Both parameters are important in mathematical models of fluid transporting epithelia (Weinstein, 1984; Weinstein, 1992).

Cell Membrane Water Permeabilities

The osmotic water permeability (P_{OSM}) of both apical and basolateral membranes of MDCK cells was low,

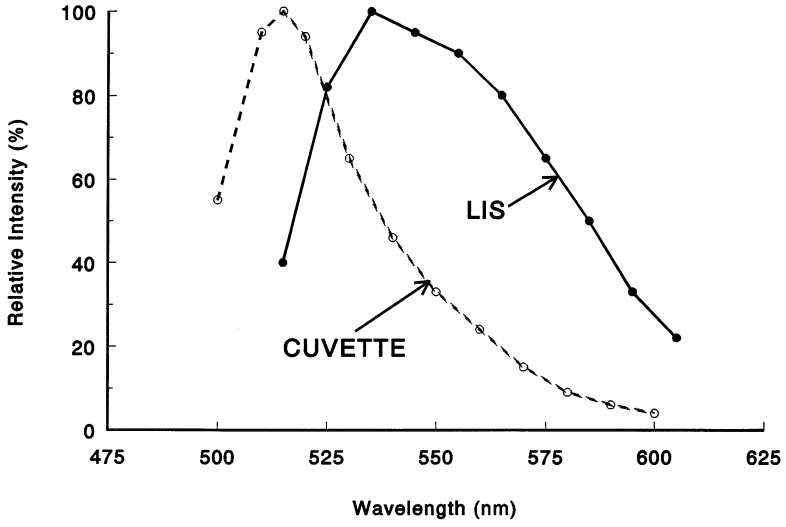

Fig. 5. Spectral scans of H-110 in a spectrofluorimeter (labeled cuvette) or within the LIS. *See* text for details.

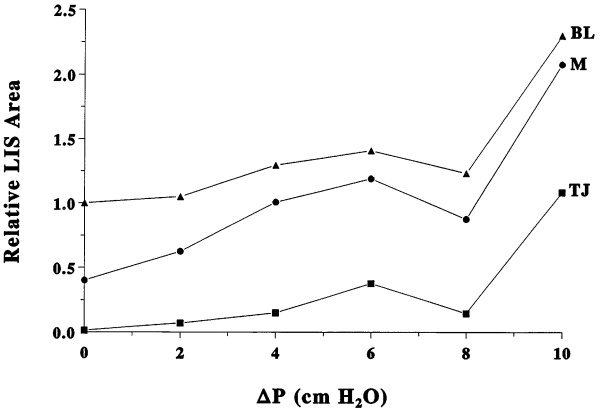

Fig. 6. Relative cross sectional area of the LIS of MDCK cell grown on permeable supports is shown as a function of the applied hydrostatic pressure difference across the epithelium. The pressure was higher in the basolateral bath compared to the apical bath (ΔP). Although optical sections were made at 1 μm intervals, only the relative areas at the level of the basolateral membrane (BL), middle of the LIS (M) and just beneath the tight junction (TJ) are shown for clarity.

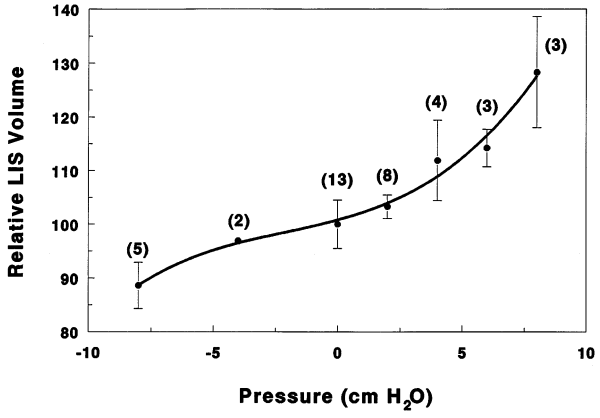

Fig. 7. The pressure-volume curve for the range of hydrostatic pressure differences is shown with the number of tissues studied in parenthesis above each point. The mean ± SEM for each point is depicted as well as the best fit polynomial (Volume $= 100.8 + 1.27P + 0.119P^2 + 0.18P^3 - 0.00008P^4$, where P is the hydrostatic pressure difference, $r = 0.992$). Fit of the compliance relation in Eq. 1 to the data from −8 to 2 cm H_2O gave a compliance of 0.05 cm H_2O^{-1}, fitting from 0 to 6 cm H_2O gave a compliance of 0.11 cm H_2O^{-1}.

comparable to that of unmodified lipid bilayers (Finkelstein, 1976). Although the apical membrane water permeability measurements seemed uninfluenced by unstirred layers (Fig. 1*A* and *B*), the unstirred layer constituted by the relatively thick permeable support clearly affected measurements of basolateral membrane water permeability made with a large osmotic gradient (Fig. 1*D*). The interference of unstirred layers on the measurement of osmotic water permeability in epithelia has been considered in detail previously (Berry, 1983) and shown to result in an underestimate of permeability. The magnitude of epithelial cell shrinkage that occurs when only one bathing solution is hypertonic also gives an indication of the relative water permeability of both cell membranes (Strange & Spring, 1987). When the apical perfusate in our experiments was 80 mOsm hypertonic, the observed shrinkage was 52% of the theoretical value (Table); when the basolateral perfusate was similarly increased, the observed shrinkage was 66% of the theoretical value. These results are consistent with the conclusion that both membranes have rather similar osmotic water permeabilities.

Although our data are the first measurements of the cell membrane water permeability of MDCK monolayers, other investigators (Mangoo-Karim & Grantham, 1990; Tanner, Maxwell & McAteer, 1992) have reported similarly low values for the P_{OSM} of MDCK cell cysts (1.2–6.8 μm/sec). Our results and those of previous in-

vestigators are consistent with the conclusion that neither the apical nor basolateral membrane of MDCK cells contain any significant quantity of water channels (aquaporins).

The low water permeability of the cell membranes might limit the rate of transepithelial fluid transport by MDCK cells. The cell membrane water permeabilities measured in the present study can be used to calculate the rate of transepithelial fluid absorption by MDCK cell monolayers. The transepithelial fluid flow, J_v, is given by:

$$J_v = \sigma L_p \Delta\pi \quad (2)$$

where L_p is the hydraulic water permeability (cm^3/cm^2-sec-mOsm/kg), σ is the solute reflection coefficient (assumed to be 1.0) and $\Delta\pi$ is the osmotic gradient (mOsm/kg). The osmotic gradient between the LIS and the apical bath is about 27.5 mOsm/kg, generated by the accumulation of ~15 mM NaCl in the LIS (Chatton & Spring, 1995). This osmotic force is exerted across the two cell membranes in series, and their series osmotic water permeability can be estimated from the data in the Table as 6.1 μm/sec. The predicted volume flow across the monolayer is 1.15 μl/cm^2-hr or 27.6 μl/cm^2 in 24 h, comparable to what has been measured in other cultured epithelia (Kersting, Kersting & Spring, 1993).

MDCK cell membrane water permeability is about 100–300 times smaller than that of the rabbit proximal straight tubule (Carpi-Medina & Whittembury, 1988) and about 125 times smaller than that of the rat proximal tubule (Green & Giebisch, 1989; Green et al., 1991). The reabsorptive fluid flow rate across the rat proximal tubule is 65×10^{-9} 1/cm^2-sec (Weinstein, 1992), about 200 times that calculated above for an MDCK monolayer.

The differences in epithelial water permeability are paralleled by the relative rates of transepithelial Na transport by the rat proximal tubule and MDCK cells. The Na transport rate of the rat proximal tubule is 9.4×10^{-9} Eq/cm^2-sec (Weinstein, 1992), 60–120 times that which can be estimated for MDCK monolayers from the single cell Na flux data of Kovbasnjuk et al. (1995). Considerable uncertainties in the MDCK epithelium Na flux estimates arise from the required assumption of a uniform apical surface area for all cells in the culture to express the Na flux per cm^2. Although the water permeability and Na transport rates of the rat proximal tubule are both about two orders of magnitude greater than those of the cultured MDCK cells, the calculated transepithelial osmotic gradient required for fluid absorption by the rat proximal tubule is 28.7 mOsm/kg (Green & Giebisch, 1989; Schafer, 1990), comparable to that measured in the MDCK cell interspace (Chatton & Spring, 1995; Xia et al., 1995).

LIS Geometry and Stability

High resolution confocal microscopic images of the LIS of MDCK cells confirmed the convoluted geometry previously reported (Harris et al., 1994). Time series studies, corrected for photobleaching of the fluorescent dye filling the LIS, failed to reveal any changes in LIS structure over sampling periods lasting up to 1 h. Little is known about the stability of cell-to-cell bridges or contacts in MDCK cells. Fluctuations of an imposed electric current flow across MDCK tight junctions has been interpreted as evidence for temporal instability of these junctions (Cerejido, Gonzalez-Mariscal & Contreras, 1989; Claude, 1978).

LIS Compliance

The compliance of the LIS of MDCK cells is about 0.05–0.11 cm H_2O^{-1} from curve fitting of the data in Fig. 7. The only other measurements of LIS compliance were made on *Necturus* gallbladder epithelium and yielded values of 0.25–0.38 cm H_2O^{-1} (Spring & Hope, 1978), indicating a much more deformable compartment than that in MDCK cells. Mathematical model calculations for the rat proximal tubule were best fit by an estimated compliance of 0.095 cm H_2O^{-1} (Weinstein, 1984) or 0.11 cm H_2O^{-1} (Huss & Marsh, 1975). The relative stiffness of MDCK cell lateral membranes may, therefore, be characteristic of renal tubular epithelial cells, and the high compliance of *Necturus* gallbladder epithelial cell membranes may not be representative of renal epithelia.

Highly deformable LIS have figured prominently in structural and electrical studies of such fluid-transporting epithelia as gallbladder and intestine. Substantial variations in LIS width as a function of transepithelial transport led previous investigators to conclude that the lateral intercellular spaces constituted the site of solute-solvent coupling (Tormey & Diamond, 1967; Whitlock & Wheeler, 1964). However, as was shown for *Necturus* gallbladder epithelium, very small transepithelial hydrostatic pressure differences can lead to dramatic changes in LIS geometry (Spring & Hope, 1978). Thus, LIS dilatation may be misleading or misinterpreted, as was reported for the rabbit cortical collecting duct (Strange & Spring, 1987). Indeed, it was pointed out by Welling and Welling (1975) that the LIS of the rabbit proximal tubule was very narrow, uniform and unlikely to be readily deformable. Our study supports the view of the MDCK LIS as a rather poorly deformable compartment compared with that of the gallbladder or intestine.

A large number of cell-to-cell bridges may provide a structural basis for the observed lateral membrane stiffness of MDCK (Wacker et al., 1992) and other renal epithelia (Zampighi & Kreman, 1985). Such bridges are

evident in our confocal images (Fig. 2) and in freeze etch electron micrographs of MDCK cells (G. Zampighi, *personal communication*). Ample cytoskeletal elements distributed along the lateral periphery of MDCK cells (Mills & Lubin, 1986) probably also provide additional stabilization of the LIS geometry. Electron microscopic studies of rabbit proximal tubule cell morphology demonstrated remarkable cell-to-cell crossbridging and uniformity of LIS width along its entire length from tight junction to cell base (Welling & Welling, 1975).

Methodological Developments

Several new approaches for fluorescence microscopy of living epithelia were developed and employed in this study. Fluorescent probes with lipid tails were evaluated for use both as membrane markers and as a strategy for introducing specific fluorophores into either the apical or basolateral cell membrane. H-110, fluorescein attached to a 14 carbon chain, proved to be suitable for basolateral membrane studies. Other investigators have used such ''float'' probes to measure near-membrane pH (Kraayenhof et al., 1993). While the utility of these probes for such near-membrane ion sensing in epithelia remains to be established, it is clear that specific labeling of one cell membrane is possible.

Spectral scanning of membrane-bound H-110 was accomplished by the use of a liquid crystal tunable filter attached to the confocal microscope. Such an arrangement had been used previously in our laboratory to determine the spectrum of BCECF within the LIS of MDCK cell monolayers (Nitschke & Spring, 1995). In the present case, the spectral shift associated with solubilization of the lipophilic probe in the lateral cell membranes was readily detectable. Spectral scanning may be of considerable future use in ascertaining the nature of the local environment of fluorescent indicator dyes.

In summary, optical microscopic methods have been further refined and utilized to measure both the cell membrane water permeability and lateral cell membrane compliance of MDCK cell monolayers.

References

Berry, C.A. 1983. Water permeability and pathways in the proximal tubule. *Am. J. Physiol.* **245:**F279–F294

Carpi-Medina, P., Whittembury, G. 1988. Comparison of transcellular and transepithelial water osmotic permeabilities (P_{OS}) in the isolated proximal straight tubule (PST) of the rabbit kidney. *Pfluegers Arch.* **412:**66–74

Cereijido, M., Gonzalez-Mariscal, L., Contreras, G. 1989. Tight junction: barrier between higher organisms and environment. *NIPS* **4:**72–75

Chatton, J.-Y., Spring, K.R. 1995. The sodium concentration of the lateral intercellular spaces of MDCK cells: a microspectrofluorimetric study. *J. Membrane Biol.* **144:**11–19

Chatton, J.-Y., Spring, K.R. 1994. Acidic pH of the lateral intercellular spaces of MDCK cells cultured on permeable supports. *J. Membrane Biol.* **140:**89–99

Claude, P. 1978. Morphological factors influencing transepithelial permeability: a model for resistance of the zonula occludens. *J. Membrane Biol.* **39:**219–232

Diamond, J.M., Bossert, W.H. 1967. Standing-gradient osmotic flow. A mechanism for coupling water and solute transport in epithelia. *J. Gen. Physiol.* **50:**2061–2083

Finkelstein, A. 1976. Water and nonelectrolyte permeability of lipid bilayer membranes. *J. Gen. Physiol.* **68:**127–135

Green, R., Giebisch, G. 1989. Reflection coefficients and water permeability in rat proximal tubule. *Am. J. Physiol.* **257:**F658–F668

Green, R., Giebsich, G., Unwin, R., Weinstein, A.M. 1991. Coupled water transport by rat proximal tubule. *Am. J. Physiol.* **261:**F1046–F1054

Harris, P.J., Chatton, J.-Y., Tran, P.H., Bungay, P.M., Spring, K.R. 1994. Optical microscopic determination of pH, solute distribution and diffusion coefficient in the lateral intercellular spaces of epithelial cell monolayers. *Am. J. Physiol.* **266:**C73–C80

Huss, R., Marsh, D.J. 1975. A model of NaCl and water flow through paracellular pathways of renal proximal tubules. *J. Membrane Biol.* **23:**305–347

Kersting, U., Kersting, D., Spring, K.R. 1993. Ketoconazole activates Cl^- conductance and blocks Cl^- and fluid absorption by cultured cystic fibrosis (CFPAC-1) cells. *Proc. Nat. Acad. Sci.* **90:**4047–4051

Kovbasnjuk, O., Chatton, J-Y., Friauf, W.S., Spring, K.R. 1995. Determination of the Na permeability of the tight junctions of MDCK cell by fluorescence microscopy. *J. Membrane Biol.* **148:**223–232

Kraayenhof, R., Sterk, G.J., Wong Fong Sang, H.W. 1993. Probing biomembrane interfacial potential and pH profiles with a new type of float-like fluorophores positioned at varying distance from the membrane surface. *Biochemistry* **32:**10057–10066

Mangoo-Karim, R., Grantham, J.J. 1990. Transepithelial water permeability in an *in vitro* model of renal cysts. *J. Am. Soc. Nephrol.* **1:**278–285

Marsh, D.J., Jensen, P.K., Spring, K.R. 1985. Computer-based determination of epithelial cell size and shape. *J. Micros.* **137:**281–292

Mills, J.W., Lubin, M. 1986. Effect of adenosine 3′,5′-cyclic monophosphate on volume and cytoskeleton of MDCK cells. *Am. J. Physiol.* **250:**C319–C324

Nitschke, R., Spring, K.R. 1995. Electro-optical wavelength selection enables confocal ratio imaging at low light levels. *J. Micros. Soc. Am.* **1:**1–11

Schafer, J.A. 1990. Transepithelial osmolality differences, hydraulic conductivities, and volume absorption in the proximal tubule. *Ann. Rev. Physiol.* **52:**709–726

Spring, K.R., Hope A. 1978. Size and shape of the lateral intercellular spaces in a living epithelium. *Science* **200:**54–58

Strange, K., Spring, K.R. 1987. Absence of significant cellular dilution during ADH-stimulated water reabsorption. *Science* **235:**1068–1070

Tanner, G.A., Maxwell, M.R., McAteer, J.A. 1992. Fluid transport in a cultured cell model of kidney epithelial cyst enlargement. *J. Am. Soc. Nephrol.* **2:**1208–1218

Tormey, J.M., Diamond, J.M. 1967. The ultrastructural route of fluid transport in rabbit gallbladder. *J. Gen. Physiol.* **50:**2031–2060

Wacker, I.U., Rickard, J.E., DeMey, J.R., Kreis, T.E. 1992. Accumulation of a microtubule-binding protein, pp170, at desmosomal plaques. *J. Cell Biol.* **117:**813–824

Weinstein, A.M. 1992. Sodium and Chloride Transport: Proximal Nephron. *In:* The Kidney: Physiology and Pathophysiology. D.W.

Seldin and G. Giebisch, editors. pp. 1925–1973. Raven Press, New York

Weinstein, A.M. 1984. Transport by epithelia with compliant lateral intercellular spaces: asymmetric oncotic effects across the rat proximal tubule. *Am. J. Physiol.* **247:**F848–F862

Welling, L.W., Welling, D.J. 1975. Surface areas of brush border and lateral cell walls in rabbit proximal nephron. *Kidney Int.* **9:**385–394

Whitlock, R.T., Wheeler, H.O. 1964. Coupled transport of solute and water across rabbit gallbladder epithelium. *J. Clin. Invest.* **48:**2249–2265

Xia, P., Persson, B.-E., Spring, K.R. 1995. The chloride concentration in the lateral intercellular spaces of MDCK cell monolayers. *J. Membrane Biol.* **144:**21–30

Zampighi, G., Kreman, M. 1985. Intercellular fibrillar skeleton in the basal interdigitations of kidney tubular cells. *J. Membrane Biol.* **88:**33–43